catalysts

MDPI

Article

Vanadium Complexes Derived from *O,N,O*-tridentate 6-bis(*o*-hydroxyalkyl/aryl)pyridines: Structural Studies and Use in the Ring-Opening Polymerization of ε-Caprolactone and Ethylene Polymerization

Mark R. J. Elsegood [1], William Clegg [2] and Carl Redshaw [3,*]

[1] Chemistry Department, Loughborough University, Loughborough LE11 3TU, UK; m.r.j.elsegood@lboro.ac.uk
[2] Chemistry, School of Natural & Environmental Sciences, Newcastle University, Newcastle upon Tyne NE1 7RU, UK; bill.clegg@ncl.ac.uk
[3] Plastics Collaboratory, Chemistry, School of Natural Sciences, University of Hull, Cottingham Road, Hull HU6 7RX, UK
* Correspondence: c.redshaw@hull.ac.uk

Abstract: Interaction of [VO(O*i*Pr)$_3$] with 6-bis(*o*-hydroxyaryl)pyridine, 2,6-{HOC(Ph)$_2$CH$_2$}$_2$(NC$_5$H$_3$), LH$_2$, afforded [VO(O*i*Pr)L] (**1**) in good yield. The reaction of LNa$_2$, generated in-situ from LH$_2$ and NaH, with [VCl$_3$(THF)$_3$] led to the isolation of [VL$_2$] (**2**) in which the pyridyl nitrogen atoms are *cis*; a regioisomer **3**·2THF, in which the pyridyl nitrogen atoms are *trans*, was isolated when using [VCl$_2$(TMEDA)$_2$]. The reaction of the 2,6-bis(*o*-hydroxyalkyl)pyridine {HOC(*i*Pr)$_2$CH$_2$}$_2$(NC$_5$H$_3$), L^{1}H$_2$, with [VO(OR)$_3$] (R = *n*Pr, *i*Pr) led, following work-up, to [VO(OR)L^1] (R = *n*Pr (**4**), *i*Pr (**5**)). Use of the bis(methylpyridine)-substituted alcohol (*t*Bu)C(OH)[CH$_2$(C$_5$H$_3$Me-5)]$_2$, L^{2}H, with [VO(OR)$_3$] (R = Et, *i*Pr) led to the isolation of [VO(μ-O)(L^2)]$_2$ (**6**). Complexes **1** to **6** have been screened for their ability to act as pre-catalysts for the ring opening polymerization (ROP) of ε-caprolactone (ε-CL), δ-valerolactone (δ-VL), and *rac*-lactide (*r*-LA) and compared against the known catalyst [Ti(O*i*Pr)$_2$L] (**I**). Complexes **1**, **4**–**6** were also screened as catalysts for the polymerization of ethylene (in the presence of dimethylaluminium chloride/ethyltrichloroacetate). For the ROP of ε-CL, in toluene solution, conversions were low to moderate, affording low molecular weight products, whilst as melts, the systems were more active and afforded higher molecular weight polymers. For δ-VL, the systems run as melts afforded good conversions, but in the case of *r*-LA, all systems as melts exhibited low conversions (<10%) except for **6** (<54%) and **I** (<39%). In the case of ethylene polymerization, the highest activity (8600 Kg·mol·V^{-1}bar^{-1}h^{-1}) was exhibited by **1** in dichloromethane, affording high molecular weight, linear polyethylene at 70 °C. In the case of **4** and **5**, which contain the propyl-bearing chelates, the activities were somewhat lower (≤1500 Kg·mol·V^{-1}bar^{-1}h^{-1}), whilst **6** was found to be inactive.

Keywords: vanadium complexes; 6-bis(*o*-hydroxyaryl)pyridine; 2,6-bis(*o*-hydroxyalkyl)pyridine; molecular structures; ring-opening polymerization; ε-CL; *r*-LA; δ-VL; ethylene polymerization

Citation: Elsegood, M.R.J.; Clegg, W.; Redshaw, C. Vanadium Complexes Derived from *O,N,O*-tridentate 6-bis(*o*-hydroxyalkyl/aryl)pyridines: Structural Studies and Use in the Ring-Opening Polymerization of ε-Caprolactone and Ethylene Polymerization. *Catalysts* **2023**, *13*, 988. https://doi.org/10.3390/catal13060988

Academic Editor: Moris S. Eisen

Received: 5 May 2023
Revised: 5 June 2023
Accepted: 6 June 2023
Published: 9 June 2023

1. Introduction

Plastics play a central role in society, and the recent COVID-19 pandemic has highlighted their continued importance [1]. Given this, there is still interest in the design of new post-metallocene systems for accessing new polyolefins, particularly as more than 60% of global plastic production is polyolefin-based [2], and partly driven by the need to generate new IP in developing countries [3]. However, petroleum-derived plastics and their subsequent disposal are problematic, and COVID-19 has only added to these problems [4]. There is, thus, also an urgent need to develop materials with greener characteristics, which can be applied to the needs of modern-day life. For example, biodegradable polymers

have seen increased use in biomedical applications [5,6], although it should be noted, too, that polyolefins have medical applications [7]. To access such polymers via either olefin polymerization or ring opening polymerization (ROP), the choice of metal employed as the catalytic centre is important, and cheap and earth-abundant metals are favourable [8–10]. We note that organic catalysts can also be used for ROP [11]. For metal-catalyzed polymerizations, including both ethylene polymerization and ROP, the ligation at the metal not only plays a significant role in determining the catalytic activity of the system but also impacts the properties of the resultant products. This versatility stems from the ability to vary the electronic and/or steric properties of the ligands, as well as improving other properties such as solubility [12–16]. With this in mind, we have been exploring the use of bulky chelating phenolates/macrocycles as ancillary ligands in both α-olefin polymerization and for the ROP of cyclic esters [17,18]. Some promising results have been achieved by combining such chelates with the metal vanadium, which is the 20th most abundant metal in the Earth's crust. In particular, we and others have found that very high catalytic activities and thermally robust systems are accessible for α-olefin polymerization when conducted in the presence of co-catalysts such as dimethylaluminium chloride and the re-activator ethyl trichloroacetate [19–31], as well as ethylene copolymerization with the likes of propylene, 1-hexene or norbonene [32–41]. Moreover, a number of vanadyl-containing systems have shown promise in the ROP of cyclic esters [42,43], whilst other systems have been shown to be promising for both ROP and α-olefin polymerization [44–49]. We also note the favourable toxicity of vanadyl complexes; for example, vanadyl sulfate is not only used as a supplement but has shown promising behaviour against Type 2 diabetes [50]. We have also shown that vanadyl calixarenes exhibit low toxicity [51]. Given this, we were interested in reports concerning the use of *O*,*N*,*O*-tridentate 6-bis(*o*-hydroxyaryl)pyridine ligation at titanium, and the use of such complexes for ethylene polymerization [52], and more recently for the ROP of ε-caprolactone (ε-CL) and *L*-lactide (*L*-LA) [53]. These titanium species exhibited only low to modest catalytic activities for ethylene polymerization (using MAO as co-catalyst), whilst, for ROP, conversions of 93 and 98% were achievable at 60 °C for ε-CL and *L*-LA, respectively. We also note that this ligand set, bound to tungsten(VI), has been employed in the *cis*-specific polymerization of norbornene [54]. Herein, we report the use of such ligation extended to vanadium-based systems (see **1**–**5**, Scheme 1), as well as structural studies, and their ability to act as catalysts for both ethylene polymerization and the ring-opening polymerization (ROP) of ε-caprolactone (ε-CL), δ-valerolactone (δ-VL), and *rac*-lactide (*r*-LA). The bis(pyridine)alkoxide (*t*Bu)C(OH)[$CH_2(C_5H_3Me\text{-}5)]_2$, whose reported coordination chemistry is somewhat limited [55,56], is also investigated (see **6**, Scheme 1).

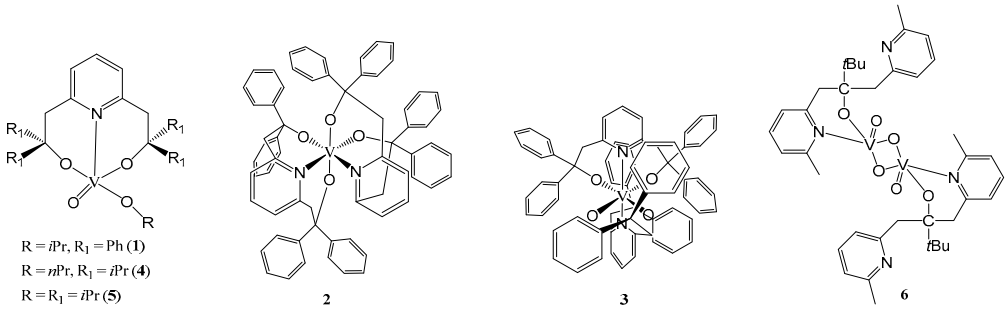

Scheme 1. Vanadium complexes **1**–**6**.

2. Results and Discussion

2.1. Synthesis and Characterization of V Complexes

2.1.1. Use of 2,6-bis(o-hydroxyaryl)pyridine, 2,6-$\{HOC(Ph)_2CH_2\}_2(NC_5H_3)$, LH_2

The reaction of 6-bis(*o*-hydroxyaryl)pyridine, 2,6-$\{HOC(Ph)_2CH_2\}_2(NC_5H_3)$, LH_2 [57], with one equivalent of $[VO(OiPr)_3]$ in refluxing toluene afforded, after workup (MeCN), yellow crystalline [VO(O*i*Pr)L] (1) in good yield. In the IR spectrum, the band at 1024 cm^{-1}

is assigned to υV=O, whilst the ^{51}V NMR spectrum (C_6D_6, 298 K) contains a single peak at δ −572.81 with $\Delta\omega_{1/2}$ 3.8 Hz. Single crystals of 1 were grown from a saturated solution in acetonitrile at ambient temperature. The molecular structure is shown in Figure 1, and selected bond lengths and angles are given in the caption. There is one molecule in the asymmetric unit. The trigonal bipyramidal vanadyl centre (τ = 0.97) [58] is chelated by the pyridine diolate ligand with the pyridyl N being axial, an oxo ligand equatorial, and an axial O*i*Pr ligand. The two diolate oxygen atoms complete the equatorial donor set. There is an intramolecular C(3)–H(3)···π{C(27)} interaction at 2.83 Å, between two Ph groups at opposite ends of the pyridine diolate ligand. In the packing, there are some weak C–H···O/π interactions.

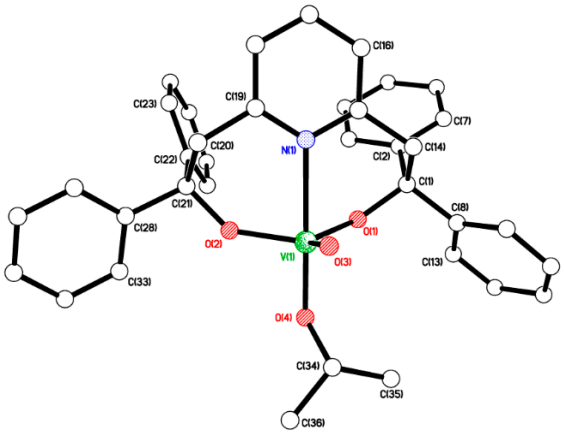

Figure 1. Molecular structure of [VO(O*i*Pr)L] (**1**). Selected bond lengths (Å) and bond angles (°): V(1)–O(1) 1.7919(15), V(1)–O(2) 1.8019(15), V(1)–O(3) 1.6089(14), V(1)–O(4) 1.7841(15), V(1)–N(1) 2.3422(18); O(1)–V(1)–O(2) 119.61(7), N(1)–V(1)–O(4) 177.51(6).

Treatment of LH_2 with two equivalents of NaH in refluxing THF and subsequent reaction with 0.5 equiv. of [VCl_3(THF)$_3$] afforded the red complex [VL_2] (**2**) in moderate yield. The molecular structure is shown in Figure 2 (left), with selected bond lengths and angles given in the caption. There is one molecule in the asymmetric unit. The complex contains a central distorted octahedral vanadium(IV) centre, and the L ligands are bound such that the pyridyl N atoms are positioned *cis*. Interestingly, the use of the vanadium(II) complex [VCl_2(TMEDA)$_2$] as starting material led, after work-up, to red crystals of **3**·2THF which were found to be a regioisomer of **2**, with the V centre on a two-fold axis and in which the pyridyl N atoms are positioned *trans* (see Figure 2, right; for an alternative view, see Figure S3, ESI).

2.1.2. Use of 2,6-bis(o-hydroxy-i-propyl)pyridine L^1H_2

Use of the related potential *O*,*N*,*O*-donor 2,6-bis(*o*-hydroxy-*i*-propyl)pyridine L^1H_2 [52] with [VO(O*n*Pr)$_3$] led, following work-up (MeCN), to the yellow complex [VO(O*n*Pr)L^1] (4). In the IR spectrum, the band at 1018 cm^{-1} is assigned to υV=O, whilst the ^{51}V NMR spectrum (C_6D_6, 298 K) contains a single peak at δ −544.70 with $\Delta\omega_{1/2}$ 2.8 Hz (see Figure S4 left, ESI). Crystals suitable for an X-ray diffraction study were grown from acetonitrile at 0 °C. The molecular structure is shown in Figure 3, with selected bond lengths and angles given in the caption. There is one molecule in the asymmetric unit. The geometry of vanadium is best described as trigonal bipyramidal, with τ 0.94 [58]. The V(1) centre lies 0.2155(6) Å out of the trigonal plane O(1)/O(2)/O(3).

Similar use of [V(O)(O*i*Pr)$_3$] with L^1H_2 afforded the complex [VO(O*i*Pr)L^1] (**5**). In the IR spectrum, the band at 1017 cm^{-1} is assigned to υV=O, whilst the ^{51}V NMR spectrum (C_6D_6, 298 K) contains a single peak at δ –572.81 with $\Delta\omega_{1/2}$ 3.8 Hz. Again, the use of acetonitrile provided crystals suitable for an X-ray diffraction study (see Figure 4). There are two very similar molecules in the asymmetric unit. The geometry exhibited at both V atoms is trigonal bipyramidal. The V(1) centre lies 0.2086(11) Å away from the equatorial

plane towards O(4), while V(2) lies 0.2228(11) Å away from the equatorial plane towards O(8). The τ value is close to 1 for both molecules [58]. Similar molecules pack in spirals along *a* with those involving V(1) in the central part of the unit cell and those involving V(2) along the *a*/*c* face (Figure 4, right).

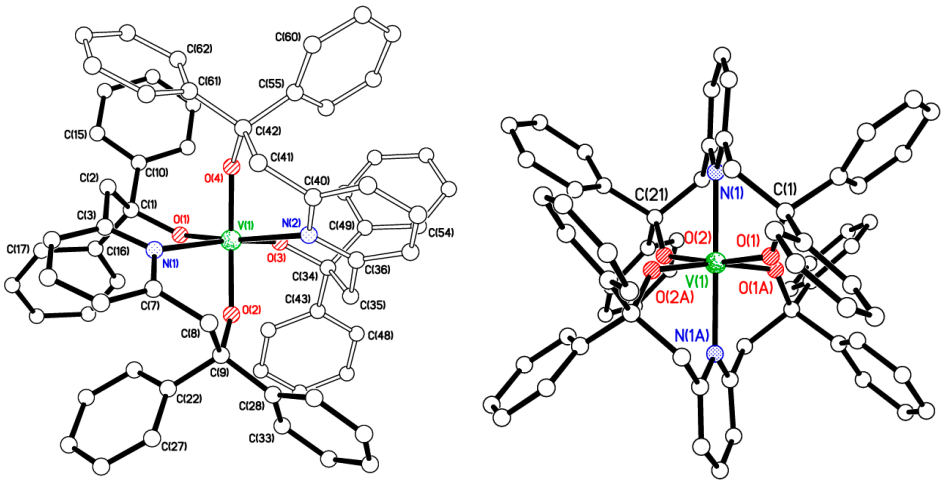

Figure 2. Left: Molecular structure of [V({OC(Ph)$_2$CH$_2$}$_2$(*cis*-NC$_5$H$_3$))$_2$] (**2**). Selected bond lengths (Å) and angles (°): V(1)–O(1) 1.8565(11), V(1)–O(2) 1.8340(10), V(1)–O(3) 1.8547(11), V(1)–O(4) 1.8230(10), V(1)–N(1) 2.2876(13), V(1)–N(2) 2.2692(13); O(2)–V(1)–O(4) 158.99(5), N(1)–V(1)–N(2) 105.87(5). **Right**: Molecular structure of [V({OC(Ph)$_2$CH$_2$}$_2$(*trans*-NC$_5$H$_3$))$_2$]·2THF (**3**·2THF). Selected bond lengths (Å) and angles (°): V(1)–O(1) 1.8819(13), V(1)–O(2) 1.8702(13), V(1)–N(1) 2.1720(16); O(1)–V(1)–O(2) 169.83(6), N(1)–V(1)–N(2) 179.68(9).

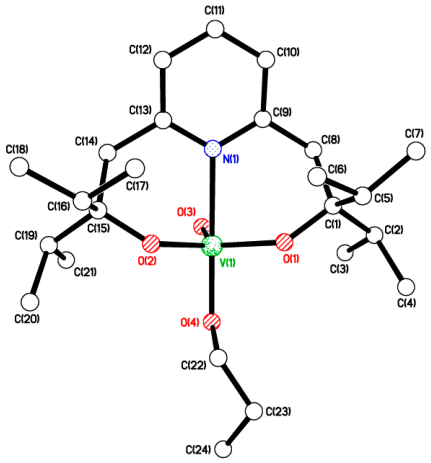

Figure 3. Molecular structure of [VO(O*n*Pr)L^1] (**4**). Selected bond lengths (Å) and angles (°): V(1)–O(1) 1.7985(9), V(1)–O(2) 1.7999(9), V(1)–O(3) 1.5984(9), V(1)–O(4) 1.8209(9), V(1)–N(1) 2.3045(11); O(1)–V(1)–O(2) 118.72(4), O(4)–V(1)–N(1) 175.13(4).

Note we have also re-determined the structure of L^{1}H$_2$ to higher precision with an *R*-factor of 0.052. It has previously been reported [52], though with a higher *R*-factor of 0.065 with CCDC refcode BAJSOX. The molecular structure is shown in Figures S1 and S2, ESI, together with details of the structure.

2.1.3. Use of the Bis(Methylpyridine)-Substituted Alcohol (tBu)C(OH)[CH$_2$(C$_5$H$_3$Me-5)]$_2$

The reaction of (*t*Bu)C(OH)[CH$_2$(C$_5$H$_3$Me-5)]$_2$ [55] with one equivalent of either [VO(OEt)$_3$] or [VO(O*i*Pr)$_3$] in refluxing toluene afforded, after workup (MeCN), yellow crystalline [VO(μ-O)(L^2)]$_2$ (**6**) in moderate yield (*ca.* 40%). In the IR spectrum, the band at 1019 cm^{-1} is assigned to *v*V=O, and the ^{51}V NMR spectrum (C$_6$D$_6$, 298 K) contains a broad

peak at δ –539.3 with $\Delta\omega_{1/2}$ 3520 Hz (see Figure S4 right, ESI). Small single crystals of **6** were grown from a saturated MeCN solution on standing for 24 h at 20 °C. The molecular structure is shown in Figure 5, with selected bond lengths and angles given in the caption. There is half a molecule in the asymmetric unit, and the molecule lies on an inversion centre. Only one of the two pyridyl nitrogen atoms binds to the metal ion from each ligand. There is approximate square-based pyramidal geometry at the V centre. The V_2O_2 diamond is fairly symmetrical, with very similar V–O bonds on each side. Pyridyl rings are not quite parallel, with a dihedral angle of 17.6° between them. This is illustrated by looking at a comparison of the distances C(5) . . . C(14) = 3.078 and C(2) . . . C(17) = 4.023 Å. The *anti*-arrangement of the Me groups on the pyridine rings is undoubtedly to minimize steric interaction. Molecules of **6** are arranged in layers with nothing unusual in terms of intermolecular interactions (see Figure S5, ESI).

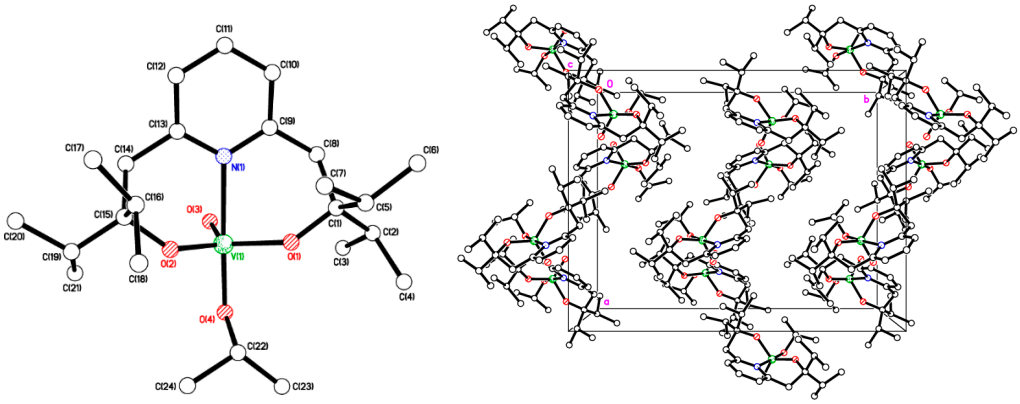

Figure 4. Left: Molecular structure of [VO(O*i*Pr)L^1] (**5**). Selected bond lengths (Å) and angles (°): V(1)–O(1) 1.8000(17), V(1)–O(2) 1.7902(16), V(1)–O(3) 1.6035(17), V(1)–O(4) 1.8097(18), V(1)–N(1) 2.285(2); O(1)–V(1)–O(2) 115.99(8), O(4)–V(1)–N(1) 177.06(7). **Right**: Packing found in **5**.

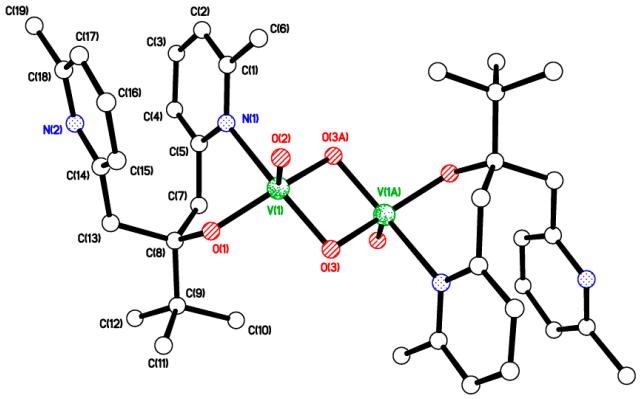

Figure 5. Molecular structure of [VO(μ-O)(L^2)]$_2$ (**6**). Selected bond lengths (Å) and angles (°): V(1)–O(1) 1.8067(9), V(1)–O(2) 1.5995(9), V(1)–O(3) 1.8214(9), V(1)–O(3A) 1.8350(9), V(1)–N(1) 2.2256(11); V(1)–O(3)–V(1A) 97.57(4), O(1)–V(1)–N(1) 83.25(4).

2.2. Ring Opening Polymerization (ROP) Studies

Complexes **1**–**6** were screened for their potential to act as catalysts for the ring-opening polymerization (ROP) of cyclic esters. Results are presented in Tables 1 and 2 (for ε-CL), Table 3 (for δ-VL), and Table 4 (for *r*-LA) and are compared against the known active catalyst [Ti(O*i*Pr)$_2$L] (**I**) [53].

Table 1. Results for ROP of ε-CL over 24 h using **1**–**6** and **I**.

Entry	Cat.	(CL):(Cat)	T/°C	Conv [a] (%)	M_n [b]	$M_{n,Cal}$ [c]	D [d]
1	**1**	500:1	15	0	-	-	-
2	**1**	500:1	60	20	270	11,430	1.63
3	**1**	500:1	90	23	380	26,270	2.10
4	**1**	500:1	130	>99	6760	56,520	2.00
5 [e]	**1**	500:1	130	>99	7610	56,520	1.67
6	**1**	100:1	130	50	550	5720	1.67
7	**1**	1000:1	130	7	250	8010	1.31
8	**1**	250:1	130	47	880	13,430	1.81
9	**2**	500:1	130	22	440	12,560	2.86
10	**3**	500:1	130	19	-	-	-
11	**4**	500:1	70	2	1275	1160	2.23
12	**4**	500:1	130	92	2510	52,520	1.35
13	**4**	100:1	130	64	270	7320	1.55
14	**5**	500:1	70	58	500	33,120	1.45
15	**5**	100:1	130	98	440	11,200	2.42
16 [e]	**5**	500:1	130	>99	4410	56,520	1.59
17	**6**	500:1	130	63	28,890/2260	35,970	1.22/1.17
18 [e]	**6**	500:1	90	49	620	27,980	1.62
19	**I**	500:1	130	>99	13,770	56,520	1.67
20 [e]	**I**	500:1	130	>99	2070	56,520	1.18

[a] Determined by ^{1}H NMR spectroscopy. [b] $M_{n/w}$, GPC values corrected considering Mark–Houwink method from polystyrene standards in THF, $M_{n/w}$ measured = 0.56 × $M_{n/w}$ GPC × 10^3. [c] Calculated from ([monomer]$_0$/[cat]$_0$) × conv (%) × monomer molecular weight (M_{CL} = 114.14) + end groups. [d] From GPC. [e] Conducted in air.

Table 2. Synthesis of polycaprolactone using complexes **1**–**6** (and **I**) as melts (130 °C, 24 h).

Entry	Cat.	(CL):(Cat)	Conv [a] (%)	M_n [b]	$M_{n,Cal}$ [c]	D [d]
1	**1**	500:1	81	5280	46,240	2.14
2 [e]	**1**	500:1	85	3090	48,530	2.06
3	**2**	500:1	83	2990	47,390	1.24
4	**3**	500:1	84	2350	47,960	1.43
5	**4**	500:1	86	2460	49,100	2.02
6 [e]	**4**	500:1	98	2080	55,950	2.92
7	**5**	500:1	>99	5960	56,520	1.17
8 [e]	**5**	500:1	>99	3460	56,520	1.09
9	**6**	500:1	>99	2270/200	56,520	1.47
10 [e]	**6**	500:1	49	3580/280	27,980	1.04
11	**I**	500:1	74	6100	42,250	2.26
12 [e]	**I**	500:1	>99	8720	56,520	1.94

[a] Determined by ^{1}H NMR spectroscopy. [b] $M_{n/w}$, GPC values corrected considering Mark–Houwink method from polystyrene standards in THF, $M_{n/w}$ measured = 0.56 × $M_{n/w}$ GPC × 10^3. [c] Calculated from ([monomer]$_0$/[cat]$_0$) × conv (%) × monomer molecular weight (M_{CL} = 114.14) + end groups. [d] From GPC. [e] Conducted in air.

Table 3. Synthesis of polyvalerolactone using complexes **1**–**6** (and **I**) as melts (130 °C, 24 h).

Entry	Cat.	[VL]:[Cat]	Conv [a] (%)	M_n [b]	$M_{n,Cal}$ [c]	D [d]
1	**1**	500:1	87	3100	43,570	1.35
2 [e]	**1**	500:1	91	920	45,570	2.00
3	**2**	500:1	77	500	38,580	1.49
4 [e]	**2**	500:1	83	330	41,570	1.27
5	**3**	500:1	75	500	49,580	1.55
6	**4**	500:1	97	3420	48,580	1.46
7 [e]	**4**	500:1	99	1550	49,580	1.87
8	**5**	500:1	89	2900	44,570	1.49

Table 3. *Cont.*

Entry	Cat.	[VL]:[Cat]	Conv [a] (%)	M_n [b]	$M_{n,Cal}$ [c]	D [d]
9 [e]	**5**	500:1	90	3990	45,070	1.18
10	**6**	500:1	75	380	37,560	1.60
11 [e]	**6**	500:1	54	390	27,050	2.16
12	**I**	500:1	72	500	36,060	1.76
13 [e]	**I**	500:1	46	360	23,050	1.85

[a] Determined by ^{1}H NMR spectroscopy. [b] $M_{n/w}$, GPC values corrected considering Mark–Houwink method from polystyrene standards in THF, $M_{n/w}$ measured = 0.57 × $M_{n/w}$ GPC × 10^3. [c] Calculated from ([monomer]$_0$/[cat]$_0$) × conv (%) × monomer molecular weight (M_{VL} = 100.16). [d] From GPC. [e] Run in air.

Table 4. Synthesis of polylactide using complexes **1**–**6** (and **I**) as melts (130 °C, 24 h).

Entry	Cat.	(*r*LA):(Cat)	Conv [a] (%)
1	**1**	500:1	3
2 [b]	**1**	500:1	2
3	**2**	500:1	3
4	**3**	500:1	1
5	**4**	500:1	10
6 [b]	**4**	500:1	8
7	**5**	500:1	8
8 [b]	**5**	500:1	1
9	**6**	500:1	43
10 [b]	**6**	500:1	54
11	**I**	500:1	29
12 [b]	**I**	500:1	39

[a] Determined by ^{1}H NMR spectroscopy. [b] Run in air.

2.2.1. ROP of ε-Caprolactone (ε-CL)

In the case of the ε-CL, for runs conducted in toluene, the products tended to be oils of low molecular weight terminated by OH groups (e.g., see Figure S6, ESI for MALDI-ToF spectra from entry 14, Table 1). Runs conducted at temperatures below 100 °C (entries **1**–**3**) resulted in poor conversion, whilst (ε-CL):(Cat) ratios either high or lower than 500:1 (entries **6**–**8**) also led to poor to moderate conversion. However, systems employing **1** under either N_2 or air at 130 °C employing the ratio 500:1 for (ε-CL:Cat) (entries **4** and **5**, respectively) and **I** under N_2 (entry **19**) afforded somewhat higher molecular weight products. A typical ^{1}H NMR spectrum of the obtained PCL is given in Figure S7, ESI. In all cases, the molecular weights of the products were still significantly lower than the theoretical values calculated via the NMR spectra. Such low molecular weights suggest that transesterification side reactions had occurred. In the case of **1** under air, the MALDI-ToF spectrum (Figure S8, ESI) revealed families of peaks terminated by either OH groups or by pyridine phenol/phenolate and OH. GPC results for dinuclear **6** under N_2 at 130 °C (entry **17**) indicated a bimodal distribution. D values range from 1.17/1.18 (for **I** and **6**), indicating good control to less controlled systems with larger D values. e.g., 2.86 (for **2**, entry **9**). Conversions were low to moderate for runs conducted at ≤90 °C or, in the case of **1**, when using a (ε-CL):(Cat) ratio other than 500:1; use of 100:1 for **5** (entry **15**) afforded a conversion of 98%. However, at 130 °C over 24 h with a ratio of 500:1, the systems employing **1**, **5**, or **I** under N_2 or air afforded > 98% conversion. Catalyst **4** also exhibited a high conversion (92%) at 130 °C under N_2 (entry **12**, Table 1). Results for coordinatively saturated **2** and **3** were similarly low, suggesting that either the *cis*/*trans* arrangement had little influence on behaviour or that, in the solution, the same regioisomer was present. Interestingly, the use of **1** (entry **5**) and **5** (entry **16**) under air led to improved performance in terms of %conversion and increased M_n, whereas the titanium catalyst **I**, whilst maintaining its %conversion, afforded a polymer of much lower molecular weight (M_n), albeit with better control (entry **20**). Kinetic studies were conducted on the structurally related complexes **1**, **4**, and **5** (see Figure 6). The results indicated the rate order was **5** > **4** > **1**, with the

logarithmic dependence appearing nonlinear, which indicates deviation from the first order in ε-CL, particularly for **1** and, to a lesser extent, **4**. This is thought to be due to these systems exhibiting induction periods. The slower performance of **1** was thought to be due to restricted access to the metal centre caused by the increased steric bulk of the phenyl groups of the pyridinediolate ligand set. We note that the use of [Ti(O*i*Pr)$_2$L] in the ROP of ε-CLin toluene at 60 °C over 20 h resulted in a conversion of 94% and a product with M_n 900 (by gpc). Use of the related complex [Ti(O*i*Pr)$_2$L^{Me}] (where L^{Me}H$_2$ = 2,2′-(4-methylpyridine-2,6-diyl)bis(1,1-diphenylethan-1-ol) afforded a similar result in toluene, but when employed as a melt at 100 °C over 8 h achieved a conversion of 99% and afforded a higher molecular weight product with M_n 5800 (by gpc) [53]. In the next section, we also employ melt conditions using **1**–**6** (and **I**).

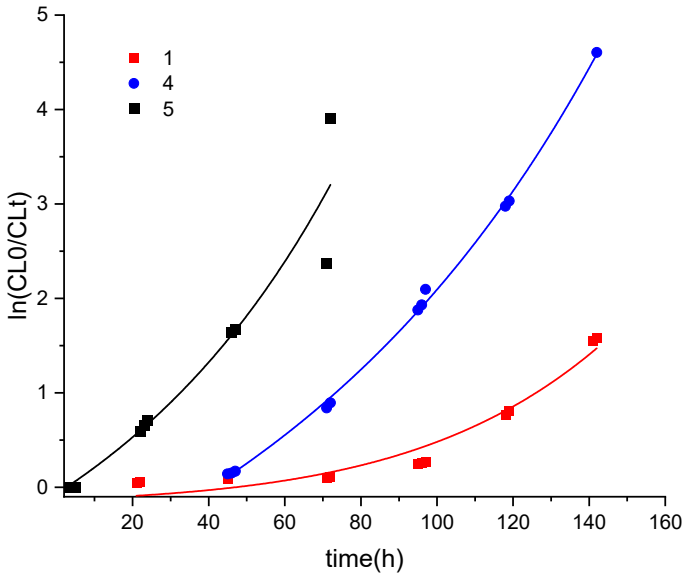

Figure 6. In(CL$_0$/CL$_t$) versus time for PCL runs using 1, 4, and 5 (500:1, 130 °C, N$_2$).

Given the varied activity, control, and generally low molecular weights achieved in the above results, the runs were also conducted in the absence of solvent, i.e., as melts, using a 500:1 ratio for (ε-CL):(Cat), see Table 2. In general, the conversions were higher, with **4**, **5,** and **I** exhibiting the highest conversions. In all cases, the molecular weights of the products were higher versus solution studies. The majority of the systems were relatively well controlled (Ds < 1.47), though the Ds for **1**, **4,** and **I** were somewhat higher (1.94–2.92). Again, the use of **6** led to bimodal behaviour (entries **9** and **10**, Table 2). End-group analysis by ^{1}H NMR spectroscopy and MALDI-ToF mass spectrometry indicated the presence of multiple products. For example, in the case of **5** under N$_2$ (Table 2, entry **7**), the MALDI-ToF spectrum contained families of peaks associated with chain polymers terminated by 2 OH or terminated by OH/O*i*Pr as well as cyclic products (Figure S9, ESI).

2.2.2. ROP of δ-Valerolactone (δ-VL)

In the case of **δ**-VL, runs were conducted as melts only (Table 3), and conversions were generally high; the lowest conversions were observed for **2** (≤83%), **3,** and **6** (≤75%), and the titanium complex I under air (46%, run **13**, Table 3). A typical ^{1}H NMR spectrum of the obtained PCL is given in Figure S10, ESI. As for PCL, molecular weights were far lower than calculated values, which was assumed to be due to transesterification; D values ranged from 1.18 to 2.16. The higher molecular weight products were afforded using complexes of the type [L/L^{1}VO(OR)], namely **1** under N$_2$, as well as **4** and **5** under either N$_2$ or air. MALDI-ToF spectra (e.g., Figures S11 and S12, ESI) of the products revealed the presence of a number of families of peaks assigned to chain polymers terminated by 2 OH groups and a smaller series assigned to cyclic polymers when using **5** as a melt under air (Table 3,

entry **6**). In the case of **5** as a melt under N_2 (Table 3, entry **7**), there were chain polymers present, terminated by OH/O*i*Pr and cyclic polymers.

2.2.3. Ring Opening Polymerization Studies of Rac-Lactide (r-LA)

In the case of the ROP of *r*-LA, runs were, again, conducted in the absence of solvent, and the results (Table 4) revealed poor conversions (<40%), except for in the case of **6** (for entry **10**, M_n = 1260 (correction factor 0.58), D 2.94). From **6**, the resulting PLA was found to be atactic (Figures S13 and S14, ESI) [59]. Given these disappointing results, the ROP of *r*-LA was not further investigated. We note that the complexes [Ti(O*i*Pr)$_2$L] and [Ti(O*i*Pr)$_2$L^{Me}] in the ROP of *L*-LA in toluene at 60 °C over **6** or 3.5 h, respectively, resulted in a conversion of 96 or 98% and afforded a product with M_n 1100 (by gpc). The use of melts with the [Ti(O*i*Pr)$_2$L^{Me}] system led to increased M_n values (>8100) with good control [53].

2.3. Ethylene Polymerization Studies

The complexes **1**, **4**, **5**, and **6** were tested, in the presence of the co-catalyst dimethylaluminium chloride (DMAC) and the re-activator trichloroethylacetate (ETA), for their ability to act as pre-catalysts for the polymerization of ethylene. The results are presented in Table 5 and reveal that the observed activities are best described as moderate in terms of vanadium-based systems [19–41]. For example, under the same conditions, the imido complexes {[V(N*p*-RC$_6$H$_4$)]$_2$L^1} (L^1 = *p*-*tert*-butyltetrahomodioxacalix [6]arene; R = CF_3, Cl, F) afforded higher activities in the range 9.0–14.8 × 10^3 Kg·molV^{-1}bar^{-1}h^{-1} [48].

Table 5. Ethylene polymerization data for homogeneous catalysts (V complex + Me_2AlCl + ETA) [a].

Complex	PE Yield, g	Average Activity Kg PE/mol V Bar h	$M\eta$ × 10^{-3}	CH_3/1000C	Double Bonds/1000C		
					888 cm^{-1}	909 cm^{-1}	965 cm^{-1}
1 [b]	1.4	2800	450	4.9	-	0.16	-
1	4.3	8600	300	0.6	-	0.10	-
4	0.6	1200	380	1.8	0.09	0.90	0.04
5	0.74	1500	360	1.1	0.11	0.13	-
6	0	0	-	-	-	-	-

[a] Polymerization conditions: V-complex (0.5 μmol) was used as a solution in 0.5 mL of CH_2Cl_2; co-catalyst (Me_2AlCl 0.5 mmol+ ETA 0.5 mmol, molar ratio V: Me_2AlCl:ETA = 1:1000:1000), dissolved in 100 mL of toluene, 100 mL of heptane; T pol 70 °C, P C_2H_4 2 bar, for 30 min. [b] **1** in 0.5 mL of toluene.

Given the poor yields, it was decided to measure M_v rather than M_w or M_n, whilst IR spectroscopy was employed to measure the methyl and C=C content; the high molecular weight and hence poor solubility of the polymers prevented the use of ^{13}C NMR spectroscopy. In all cases, the systems afforded high molecular weight linear polyethylene with a methyl branch content ≤4.9 per 1000 carbons.

In the case of complex **1**, the best results were obtained upon its introduction into the reactor as the solution in CH_2Cl_2 rather than in toluene, presumably as a result of increased solubility. If the groups bound to the carbon atoms adjacent to oxygen in the chelate are changed to a less bulky propyl group, then the activity is reduced from 8600 Kg·molV^{-1}bar^{-1}h^{-1} in **1** (bearing phenyl substituents) to 1200 Kg·molV^{-1}bar^{-1}h^{-1} for **4** (bearing *n*-propyl substituents) and to 1500 Kg·molV^{-1}bar^{-1}h^{-1} for **5** (bearing *n*-propyl substituents). Surprisingly, similar use of **6** led to inactivity, and this is tentatively assigned to the unfavourable flexibility of the free methylpyridine-containing arm, which has the potential to block access to the metal. The active species in these systems is thought to be a paramagnetic species formed on the reduction of the metal centre by the excess co-catalyst. We and others have investigated such species in related systems [60–63].

3. Materials and Methods

3.1. General

All reactions were conducted under an inert atmosphere using standard Schlenk techniques. Toluene was dried from sodium, acetonitrile was distilled from calcium hydride, and all solvents were degassed prior to use. IR spectra (nujol mulls, KBr windows) were recorded on a Nicolet Avatar 360 FTIR spectrometer, NMR spectrometer 400.2 MHz on a JEOL ECZ 400S spectrometer, with TMS δH = 0 as the internal standard or residual protic solvent [CD_3CN, δH = 1.94]. ^{51}V NMR spectra were recorded from C_6D_6 solutions at 105.1 MHz, ^{51}V chemical shifts were referenced to external $VOCl_3$ sample. Chemical shifts are given in ppm (δ), and coupling constants (*J*) are given in Hertz (Hz). Elemental analyses were performed by the elemental analysis service at the Department of Chemistry, the University of Hull, or London Metropolitan University. FTIR spectra (nujol mulls, KBr windows) were recorded on a Nicolet Avatar 360 FT-IR spectrometer. Matrix-Assisted Laser Desorption/Ionization Time of Flight (MALDI-TOF) mass spectrometry was performed in a Bruker autoflex III smart beam in linear mode, and the spectra were acquired by averaging at least 100 laser shots. 2,5-Dihydroxybenzoic acid was used as the matrix, and THF was used as a solvent. Sodium chloride was dissolved in methanol and used as the ionizing agent. Samples were prepared by mixing 20 μL of matrix solution in THF (2 mg·mL^{-1}) with 20 μL of matrix solution (10 mg·mL^{-1}) and 1 μL of a solution of ionizing agent (1 mg·mL^{-1}). Then, 1 mL of these mixtures was deposited on a target plate and allowed to dry in air at ambient temperature. The known compounds LH_2, L^1H_2, L^2H, $[VCl_3(THF)_3]$ and $[VCl_2(TMEDA)_2]$ were prepared by the literature methods [52,55,57,64,65]. The reagents $[VO(OR)_3]$ (R = *n*Pr, *i*Pr) were purchased from Sigma Aldrich and were used as received. Molecular weights were calculated from the experimental traces using the OmniSEC software.

Crystal structures were determined from data collected at the UK National Crystallography Service (**1**, **2**, **4**–**6**) and in the home laboratory for **3**. Full details are given in the ESI. Crystal data are summarized in Tables S1 and S2.

*3.2. Preparation of [VO(OiPr)L] (**1**)*

To $[VO(OiPr)_3]$ (0.50 mL, 2.12 mmol) and LH_2 (1.00 g, 2.12 mmol) was added toluene (30 mL), and then the system was refluxed for 12 h. On cooling, the volatiles were removed in a vacuo, and the residue was extracted into warm MeCN (30 mL). Yield: 1.09 g, 87%. $C_{36}H_{34}NO_4V$ requires C 72.59, H 5.75, and N 2.35%. Found: C 72.50, H 5.84, N 2.06%. IR: 1599 m, 1576 m, 1319 m, 1259 s, 1239 m, 1209 w, 1175 w, 1110 s, 1091 s, 1057 s, 1024 s, 956 s, 914 m, 892 m, 854 m, 813 m, 790 m, 765 w, 736 w, 704 s, 694 s, 669 w, 650 m, 620 w, 600 m, 532 w, 507 m, 486 m, 454 w. ^1H NMR (C_6D_6) δ: 7.69 (d, *J* = 7.6 Hz, 4 H, aryl*H*), 7.19 (m, 8 H, aryl*H*), 7.06 (m, 2 H, aryl*H*), 6.87 (overlapping m, 6 H, aryl*H*), 6.42 (t, *J* = 7.6 Hz,1 H, aryl*H*), 6.12 (d, *J* = 7.6 Hz, 2 H, aryl*H*), 6.02 (sept, *J* = 6.0 Hz, 1 H, C*H*Me$_2$), 4.22 (d, *J* = 14.4 Hz, 2 H, CH_2), 3.47 (d, *J* = 14.4 Hz, 2 H, CH_2), 1.36 (d, *J* = 6.0 Hz, 6 H, CH*Me*$_2$). ^{51}V (C_6D_6) δ: −572.09 ($\Delta\omega_{1/2}$ = 4 Hz).

*3.3. Preparation of [V({OC(Ph)$_2$CH$_2$}$_2$(cis-NC$_5$H$_3$))$_2$] (**2**)*

To LH_2 (1.00 g, 2.12 mmol) in THF (30 mL) was added NaH (0.10 g, 4.17 mmol), and the system was refluxed for 12 h. On cooling (to −78 °C), $[VCl_3(THF)_3]$ (0.40 g, 1.07 mmol) was added, and the system was stirred for 12 h. The system was filtered, concentrated to about 20 mL, and left to stand at 0 °C to afford red crystals of **2**. Yield: 0.58 g, 55%. $C_{66}H_{54}N_2O_4V$ requires C 80.06, H 5.50, and N 2.83%. Found: C 80.51, H 5.55, N 2.80%. IR: 1975 w, 1886 w, 1815 w, 1667, 1601 m, 1579 w, 1317 m, 1261 s, 1151 m, 1097 s, 1021 s, 940 m, 918 w, 800 s, 722 m, 700 s, 639 w, 594 w, 547 w, 522 w, 492 w, 467 w. M.S. (MALDI): 836 (M—2Ph).

*3.4. Preparation of [V({OC(Ph)$_2$CH$_2$}$_2$(trans-NC$_5$H$_3$))$_2$] (**3**·2THF)*

As for **2**, but using [VCl$_2$(TMEDA)$_2$] (0.38 g, 1.07 mmol), LH$_2$ (1.00 g, 2.12 mmol) and NaH (0.10 g, 4.17 mmol) afforded **3**·2THF as red prisms. Yield: 0.45 g, 37%. $C_{74}H_{70}N_2O_6V$—THF (sample dried in vacuo for 1 h) requires C 79.15, H 5.88, N 2.63%. Found: C 79.46, H 6.02, N 2.33%. IR: 1667 w, 1631 w, 1601 w, 1551 w, 1413 m, 1304 m, 1261 s, 1094 bs, 1020 bs, 940 w, 918 w, 865 w, 800 s, 722 m, 700 m, 639 w, 598 w, 466 w.

*3.5. Preparation of [VO(OnPr)L^1] (**4**)*

To [VO(O*n*Pr)$_3$] (0.68 mL, 3.00 mmol) and L^{1}H$_2$ (1.00 g, 2.98 mmol) was added toluene (30 mL), and then the system was refluxed for 12 h. On cooling, the volatiles were removed in vacuo, and the residue was extracted into warm MeCN (30 mL). On cooling to −20 °C, golden brown crystals of **4** formed. Yield: 0.89 g, 65%. $C_{24}H_{42}NO_4V$ requires C 62.73, H 9.21, and N 3.05%. Found: C 62.37, H 9.61, N 3.29%. IR: 2008 w, 1599 m, 1575 m, 1331 m, 1261 s, 1234 w, 1177 m, 1138 m, 1094 s, 1063 s, 1018 s, 981 s, 964 s, 913 w, 901 m, 863 w, 800 s, 772 m, 723 w, 708 m, 684 w, 658 m, 640 s, 628 s, 559 s, 494 w, 450 s, 410 s. ^{1}H NMR (C_6D_6) δ: 7.10 (1 H, aryl*H*), 6.82 (1 H, aryl*H*), 6.42 (1 H, aryl*H*), 5.20 (t, *J* = 6.4 Hz, 2 H, OC*H*$_2$), 3.62 (d, *J* = 14.0 Hz, 2 H, C*H*$_2$), 2.61 (d, *J* = 14.4 Hz, 2 H, C*H*$_2$), 2.05 (sept, *J* = 6.8 Hz, C*H*Me$_2$), 1.83 (m, *J* = 7.2 Hz, 2 H, OCH$_2$C*H*$_2$CH$_3$), 1.71 (sept, *J* = 6.8 Hz, C*H*Me$_2$), 1.25 (d, *J* = 6.8 Hz, 6 H, CH*Me*$_2$), 1.16 (d, *J* = 6.8 Hz, 6 H, CH*Me*$_2$), 1.05 (t, *J* = 7.2 Hz, 3 H, OCH$_2$CH$_2$C*H*$_3$), 0.76 (d, *J* = 6.8 Hz, 6 H, CH*Me*$_2$), 0.62 (d, *J* = 6.8 Hz, 6 H, CH*Me*$_2$). ^{51}V (C_6D_6) δ: −544.70 ($\Delta\omega_{1/2}$ = 2.8 Hz).

*3.6. Preparation of [VO(OiPr)L^1] (**5**)*

To [VO(O*i*Pr)$_3$] (0.71 mL, 3.01 mmol) and L^{1}H$_2$ (1.00 g, 2.98 mmol) was added toluene (30 mL), and then the system was refluxed for 12 h. On cooling, the volatiles were removed in vacuo, and the residue was extracted into warm MeCN (30 mL). On cooling to −20 °C, yellow crystals of **5** formed. Yield: 1.17 g, 85%. $C_{24}H_{42}NO_4V$ requires C 62.73, H 9.21, and N 3.05%. Found: C 61.92, H 9.55, N 3.16%.* IR: 1993 w, 1599 m, 1574 m, 1317 m, 1261 m, 1231 w, 1203 w, 1165 m, 1137 m, 1105 s, 1017 s, 972 s, 943 s, 905 m, 866 w, 838 m, 815 m, 770 m, 721 m, 705 m, 645 s. ^{1}H NMR (C_6D_6) δ: 6.93 (bm, 1 H, aryl*H*), 6.51 (bd, 2 H, aryl*H*), 5.73 (sept, *J* = 6.8 Hz, 1 H, C*H*Me$_2$), 3.61 (d, *J* = 14.4 Hz, 2 H, C*H*$_2$), 2.62 (d, *J* = 14.4 Hz, 2 H, C*H*$_2$), 2.06 (br sept, *J* = 6.0 Hz, 2 H, C*H*Me$_2$), 1.68 (sept, *J* = 6.8 Hz, 2 H, C*H*Me$_2$), 1.44 (d, *J* = 6.8 Hz, 6 H, CH*Me*$_2$), 1.26 (d, *J* = 6.8 Hz, 6 H, CH*Me*$_2$), 1.13 (d, *J* = 6.8 Hz, 6 H, CH*Me*$_2$), 0.74 (d, *J* = 6.8 Hz, 6 H, CH*Me*$_2$), 0.62 (d, *J* = 6.8 Hz, 6 H, CH*Me*$_2$). ^{51}V (C_6D_6) δ: −572.81 ($\Delta\omega_{1/2}$ = 3.8 Hz). *Despite repeated attempts, this was the best fit for elemental analysis.

*3.7. Preparation of [VO(μ-O)(L^2)]$_2$ (**6**)*

To [VO(O*i*Pr)$_3$] (0.79 mL, 3.35 mmol) and L^{2}H (1.00 g, 3.35 mmol) was added toluene (30 mL), and then the system was refluxed for 12 h. On cooling, the volatiles were removed in vacuo, and the residue was extracted into warm MeCN (30 mL). On cooling to −20 °C, small yellow crystals of **6** formed. Yield: 0.52 g, 41%. $C_{38}H_{50}N_4O_6V_2$ requires C 59.99, H 6.63, and N 7.37%. Found: C 60.70, H 7.07, N 7.45%. IR: 1639 w, 1593 s, 1578 s, 1304 m, 1261 s, 1203 w, 1155 m, 1097 s, 1019 s, 862 w, 794 s, 765 m, 666 w, 614 w, 581 w, 504 w. ^{1}H NMR (CD_3CN) δ: 7.47 (t, 4 H, *J* = 7.6 Hz, aryl*H*), 7.03 (d, 4 H, *J* = 7.6 Hz, aryl*H*), 6.91 (d, 4 H, *J* = 7.4 Hz, aryl*H*), 3.00 (s, 8 H, C*H*$_2$), 2.33 (s, 12 H, C*H*$_3$), 0.97 (s, 18 H, C(C*H*$_3$)$_3$). ^{51}V (C_6D_6) δ: −539.3 ($\Delta\omega_{1/2}$ = 3520 Hz). Complex **5** is also available via the use of [VO(OEt)$_3$].

3.8. Procedure for ROP of ε-Caprolactone

A toluene solution of pre-catalyst (0.010 mmol, 1.0 mL toluene) was introduced into a Schlenk tube in the glove box at room temperature. The solution was stirred for 2 min, and then the appropriate equivalent of BnOH (from a pre-prepared stock solution of 1 mmol BnOH in 100 mL toluene) and the appropriate amount of ε-CL along with 1.5 mL toluene were added to the solution. For example, for Table 2, entry 1, a toluene solution of pre-

catalyst **1** (0.010 mmol, 1.0 mL toluene) was introduced into a Schlenk tube, then 2 mL BnOH solution (1 mmol BnOH/100 mL toluene) and 20 mmol ε-CL along with 1.5 mL toluene was added to the solution. The reaction mixture was then placed into an oil/sand bath pre-heated at 130 °C, and the solution was stirred for the prescribed time (8 or 24 h). The polymerization mixture was quenched with the addition of an excess of glacial acetic acid (0.2 mL) to the solution, and the resultant solution was then poured into methanol (200 mL). The resultant polymer was then collected on filter paper and dried in vacuo.

3.9. Kinetic Studies

The polymerizations were carried out at 130 °C in toluene (2 mL) using 0.010 mmol of the complex. The molar ratio of monomer to initiator was fixed at 500:1, and at appropriate time intervals, 0.5 μL aliquots were removed (under N_2) and were quenched with wet $CDCl_3$. The percentage conversion of monomer to polymer was determined using ^{1}H NMR spectroscopy.

3.10. Procedure for Ethylene Polymerization

Ethylene polymerization experiments were performed in a steel 500 mL autoclave. The reactor was evacuated at 80 °C, cooled to 20 °C, and then charged with the freshly prepared solution of the co-catalyst in heptane/toluene. Pre-catalysts were introduced into the reactor in sealed glass ampoules containing 0.5 or 1.0 μmol of appropriate V-complex in 0.5 mL of solvent. After setting up the desired temperature and ethylene pressure, the reaction was started by breaking the ampoule with the pre-catalyst. During the polymerization, ethylene pressure (2 bar), temperature (70 °C), and stirring speed (2000 rpm) were maintained constant. After 30 min (during which time the ethylene consumption rate declined to nearly zero level), the reactor was opened to the atmosphere, and the polymeric product was dried in a fume-hood to a constant weight.

Polymerization conditions. For entry 1 of Table 5: V loading 1.0 μmol (dissolved in CH_2Cl_2), co-catalyst Et_2AlCl + ETA (molar ratio V: Et_2AlCl:ETA = 1:1000:500) in 50 mL of toluene + 100 mL of heptane, T pol 70 °C, P C_2H_4 = 2 bar, for 30 min. For entries 2–8 of Table 5: V complex was dissolved in toluene, co-catalyst Me_2AlCl + ETA (molar ratio V:Me_2AlCl:ETA = 1:1000:1000) in 100 mL of toluene + 100 mL of heptane; T pol 70 °C, P C_2H_4 = 2 bar, for 30 min.

4. Conclusions

The products resulting from the interaction of the potentially *O*,*N*,*O*-tridentate 6-bis(*o*-hydroxyaryl)pyridines 2,6-{$HOC(X)_2CH_2$}$_2$(NC_5H_3) (X = Ph, LH_2; *i*Pr, L^1H_2) with the vanadyl trisalkoxides [$VO(OR)_3$] (R = *n*-Pr, *i*-Pr) have been isolated in good yield and characterized as [VO(O*i*/*n*-Pr)L/L^1]. The use of LNa_2 with [$VCl_3(THF)_3$] afforded [VL_2] in which the pyridyl N atoms are positioned *cis*, whereas the use of [$VCl_2(TMEDA)_2$] afforded the regioisomer with *trans* pyridine rings. The related potentially *N*,*O*,*N*-tridentate bis(methylpyridine)-substituted alcohol (*t*Bu)C(OH)[$CH_2(C_5H_3Me\text{-}5)]_2$, L^2H, on treatment with [$VO(OR)_3$] (R = Et, *i*-Pr) afforded [VO(μ-O)(L^2)]$_2$, in which L^2 binds in *N*,*O*-bidentate fashion. These products were screened for their ability to act as catalysts for the ring-opening polymerization of ε-caprolactone (ε-CL), δ-valerolactone (δ-VL), and *rac*-lactide (*r*-LA). In the case of ε-CL, products formed in solution were both linear and cyclic and of low molecular weight. Higher molecular weight products were formed when melt conditions were employed. In the case of δ-VL, linear and cyclic products were also formed, with the higher molecular weight products accessed when using systems employing [L/L^1VO(OR)], i.e., **1**, **4**, and **5**. For both PCL and PVL, the low molecular weights (versus the theoretical values) suggested transesterifaction side reactions had occurred. For *r*-LA, only the bis(methylpyridine)-substituted alcohol-derived complex **6** exhibited any appreciable activity. Complexes **1**, **4**, and **5** displayed moderate activities in ethylene polymerization in the presence of dimethylaluminium chloride (DMAC) activator and the

re-activator trichloroethylacetate (ETA), affording linear high-MW polyethylene, whilst **6** was inactive under the conditions.

Supplementary Materials: The following supporting information can be downloaded at: https://www.mdpi.com/article/10.3390/catal13060988/s1, Figure S1: Molecular structure of L^1H_2; Figure S2: Intermolecular interaction and packing of L^1H_2; Figure S3: Alternative view of the molecular structure of $V(\{OC(Ph)_2CH_2\}_2(trans\text{-}NC_5H_3))_2]\cdot 2THF$ (**3**·2THF); Packing of **6**; Table S1: Crystallographic data for **1**, **2** and **3**·2THF; Table S2: Crystallographic data for **4**–**6** and L^1H_2; Figure S4: ^{51}V NMR spectra of **4** and **6**; Figure S5: Packing of **6**; Figure S6: MALDI-ToF of PCL using **5** under N_2 at 70 °C (entry 14, Table 1); Figure S7: ^1H NMR spectrum of PCL (using 1 in air, entry 5, Table 1); Figure S8: MALDI-ToF of PCL using **1** under air (entry 5, Table 1); Figure S9: MALDI-ToF of PCL using **5** as a melt under N_2 (entry 7, Table 2); Figure S10: ^1H NMR spectrum of PVL (using **4** under N_2, entry 6, Table 3); Figure S11: MALDI-ToF of PVL using **5** as a melt under air (entry 8, Table 3); Figure S12: MALDI-ToF of PVL using **5** as a melt under N_2 (entry 9,Table 3); Figure S13: ^{13}C NMR spectrum of the methine region of the PLA using **6** under N_2 (entry 9, Table 4); Figure S14: ^{13}C NMR spectrum of the methine region of the PLA using **6** under air (entry 10, Table 4) [66,67].

Author Contributions: M.R.J.E. formal analysis; W.C. formal analysis; C.R. conceptualization, funding acquisition, writing—review and editing. All authors have read and agreed to the published version of the manuscript.

Funding: The EPSRC National X-ray Crystallography Service (Southampton) is thanked for data collection. CR also thanks the British Council for funding a workshop, and the EPSRC (grant number EP/S025537/1) for funding.

Data Availability Statement: The supplementary crystallographic data can be found free of charge at the Cambridge Crystallographic Data Centre. Deposition numbers 2239107-2239113.

Acknowledgments: We thank the EPSRC National Crystallographic Service at Southampton for data collection. We thank the British Council Newton Fund for support. We thank V.C. Gibson (Imperial College) for the use of the synthesis of **3**.

Conflicts of Interest: The authors declare no conflict of interest. The funders had no role in the design of the study; in the collection, analyses, or interpretation of data; in the writing of the manuscript, or in the decision to publish the results.

References

1. Czigany, T.; Ronkay, F. The coronavirus and plastics. *Express Polym. Lett.* **2020**, *14*, 510–511. [CrossRef]
2. Jehanno, C.; Alty, J.W.; Roosen, M.; De Meester, S.; Dove, A.P.; Chen, E.Y.-X.; Leibfarth, F.A.; Sardon, H. Critical advances and future opportunities in upcycling commodity polymers. *Nature* **2022**, *603*, 803–814. [CrossRef] [PubMed]
3. Reichman, J.H. Intellectual Property in the Twenty-First Century: Will the Developing Countries Lead or Follow? In *Intellectual Property Rights: Legal and Economic Challenges for Development*; Cimoli, M., Dosi, G., Maskus, K.E., Okediji, R.L., Reichman, J.H., Eds.; Oxford University Press: Oxford, UK, 2014. [CrossRef]
4. Silva, A.L.P.; Prata, J.C.; Duarte, A.C.; Barcelò, D.; Rocha-Santos, T. An urgent call to think globally and act locally on landfill disposable plastics under and after COVID-19 pandemic: Pollution prevention and technological (Bio) remediation solutions. *Chem. Eng. J.* **2021**, *426*, 131201. [CrossRef] [PubMed]
5. Albertsson, A.-C.; Varma, I.K. Recent Developments in Ring Opening Polymerization of Lactones for Biomedical Applications. *Biomacromolecules* **2003**, *4*, 1466–1486. [CrossRef]
6. Tian, H.; Tang, Z.; Zhuang, X.; Chen, X.; Jing, X. Biodegradable Synthetic Polymers: Preparation, functionalization and biomedical application. *Prog. Polym. Sci.* **2012**, *37*, 237–280. [CrossRef]
7. Kim, Y.K. The use of polyolefins in industrial and medical applications. In *The Textile Institute Book Series, Polyolefin Fibres*, 2nd ed.; Woodhead Publishing: Sawston, UK, 2017; pp. 135–155. ISBN 9780081011324. [CrossRef]
8. Arbaoui, A.; Redshaw, C. Metal Catalysts for ε-caprolactone polymerisation. *Polym. Chem.* **2010**, *1*, 801–826. [CrossRef]
9. Zhang, X.; Fevre, M.; Jones, G.O.; Waymouth, R.M. Catalysis as an Enabling Science for Sustainable Polymers. *Chem. Rev.* **2018**, *118*, 839–885. [CrossRef]
10. Chen, C. Designing catalysts for olefin polymerization and copolymerization: Beyond electronic and steric tuning. *Nat. Rev. Chem.* **2018**, *2*, 6–14. [CrossRef]
11. Dove, A.P. Organic Catalysis for Ring-Opening Polymerization. *ACS Macro Lett.* **2012**, *1*, 1409–1412. [CrossRef]
12. Kamber, N.E.; Jeong, W.; Waymouth, R.M.; Pratt, R.C.; Lohmeijer, B.G.G.; Hedrick, J.L. Organocatalytic Ring-Opening Polymerization. *Chem. Rev.* **2007**, *107*, 5813–5840. [CrossRef]

13. Williams, C.K.; Hillmyer, M.A. Polymers from Renewable Resources: A Perspective for a Special Issue of Polymer Reviews. *Polym. Rev.* **2008**, *48*, 1–10. [CrossRef]
14. Place, E.S.; George, J.H.; Williams, C.K.; Stevens, M.M. Synthetic Polymer Scaffolds for Tissue Engineering. *Chem. Soc. Rev.* **2009**, *38*, 1139–1151. [CrossRef]
15. Labet, M.; Thielemans, W. Synthesis of Polycaprolactone: A review. *Chem. Soc. Rev.* **2009**, *38*, 3484–3504. [CrossRef]
16. Lecomte, P.; Jér, C. *Synthetic Biodegradable Polymers*; Rieger, B., Künkel, A., Coates, G., Reichardt, R., Dinjus, E., Zevaco, T., Eds.; Springer: Berlin/Heidelberg, Germany, 2011; Volume 245, pp. 173–211. ISBN 978-3642271533.
17. Redshaw, C. Metallocalixarene catalysts: α-olefin polymerization and ROP of cyclic esters. *Dalton Trans.* **2016**, *45*, 9018–9030. [CrossRef]
18. Redshaw, C. Use of Metal Catalysts Bearing Schiff Base Macrocycles for the Ring Opening Polymerization (ROP) of Cyclic Esters. *Catalysts* **2017**, *7*, 165. [CrossRef]
19. Redshaw, C.; Warford, L.; Dale, S.H.; Elsegood, M.R.J. Vanadyl complexes bearing bi- and triphenolate chelate ligands: Highly active ethylene polymerisation procatalysts. *Chem. Commun.* **2004**, 1954–1955. [CrossRef]
20. Redshaw, C.; Rowan, M.A.; Homden, D.M.; Dale, S.H.; Elsegood, M.R.J.; Matsui, S.; Matsuura, S. Vanadyl C and N-capped tris(phenolate) complexes: Influence of pro-catalyst geometry on catalytic activity. *Chem. Commun.* **2006**, 3329–3331. [CrossRef]
21. Redshaw, C.; Rowan, M.A.; Warford, L.; Homden, D.M.; Arbaoui, A.; Elsegood, M.R.J.; Dale, S.H.; Yamato, T.; Casas, C.P.; Matsui, S.; et al. Oxo- and Imidovanadium Complexes Incorporating Methylene- and Dimethyleneoxa-Bridged Calix[3]- and -[4]arenes: Synthesis, Structures and Ethylene Polymerisation Catalysis. *Chem.-Eur. J.* **2007**, *13*, 1090–1107. [CrossRef]
22. Homden, D.; Redshaw, C.; Warford, L.; Hughes, D.L.; Wright, J.A.; Dale, S.H.; Elsegood, M.R.J. Synthesis, structure and ethylene polymerisation behaviour of vanadium(iv and v) complexes bearing chelating aryloxides. *Dalton Trans.* **2009**, 8900–8910. [CrossRef]
23. Lorber, C.; Despagnet-Ayoub, E.; Vendier, L.; Arbaoui, A.; Redshaw, C. Amine influence in vanadium-based ethylene polymerisation pro-catalysts bearing bis(phenolate) ligands with 'pendant' arms. *Catal. Sci. Technol.* **2011**, *1*, 489–494. [CrossRef]
24. Nomura, K.; Zhang, S. Design of Vanadium Complex Catalysts for Precise Olefin Polymerization. *Chem. Rev.* **2011**, *111*, 2342–2362. [CrossRef] [PubMed]
25. Wu, J.-Q.; Li, Y.-S. Well-defined vanadium complexes as the catalysts for olefin polymerization. *Coord. Chem. Rev.* **2011**, *255*, 2303–2314. [CrossRef]
26. Ma, J.; Zhao, K.-Q.; Walton, M.J.; Wright, J.A.; Frese, J.W.A.; Elsegood, M.R.J.; Xing, Q.; Sun, W.-H.; Redshaw, C. Vanadyl complexes bearing bi-dentate phenoxyimine ligands: Synthesis, structural studies and ethylene polymerization capability. *Dalton Trans.* **2014**, *43*, 8300–8310. [CrossRef]
27. Phillips, A.M.F.; Suo, H.; Silva, M.D.F.C.G.D.; Pombeiro, A.J.; Sun, W.-H. Recent developments in vanadium-catalyzed olefin coordination polymerization. *Coord. Chem. Rev.* **2020**, *416*, 213332. [CrossRef]
28. Qian, J.; Comito, R.J. A Robust Vanadium(V) Tris(2-pyridyl)borate Catalyst for Long-Lived High-Temperature Ethylene Polymerization. *Organometallics* **2021**, *40*, 1817–1821. [CrossRef]
29. Wu, R.; Niu, Z.; Huang, L.; Xia, Z.; Feng, Z.; Qi, Y.; Dai, Q.; Cui, L.; He, J.; Bai, C. Vanadium complexes bearing the bulky bis(imino)pyridine ligands: Good thermal stability toward ethylene polymerization. *Eur. Polym. J.* **2022**, *180*, 111569. [CrossRef]
30. Suo, H.; Phillips, A.M.F.; Satrudhar, M.; Martins, L.M.D.R.S.; Silva, M.d.F.G.d.; Pombeiro, A.J.L.; Han, M.; Sun, W. Achieving ultra-high molecular weight polyethylenes by vanadium aroylhydrazine-arylolates. *J. Polym. Sci.* **2023**, *61*, 482–490. [CrossRef]
31. Qian, J.; Comito, R.J. Ethylene Polymerization with Thermally Robust Vanadium(III) Tris(2-pyridyl)borate Complexes. *Organometallics* **2023**. [CrossRef]
32. Homden, D.M.; Redshaw, C.; Hughes, D.L. Vanadium Complexes Possessing $N_2O_2S_2$-Based Ligands: Highly Active Procatalysts for the Homopolymerization of Ethylene and Copolymerization of Ethylene/1-hexene. *Inorg. Chem.* **2007**, *46*, 10827–10839. [CrossRef]
33. Redshaw, C.; Walton, M.; Michiue, K.; Chao, Y.; Walton, A.; Elo, P.; Sumerin, V.; Jiang, C.; Elsegood, M.R.J. Vanadyl calix[6]arene complexes: Synthesis, structural studies and ethylene homo-(co-)polymerization capability. *Dalton Trans.* **2015**, *44*, 12292–12303. [CrossRef]
34. Redshaw, C.; Walton, M.J.; Elsegood, M.R.J.; Prior, T.J.; Michiue, K. Vanadium(v) tetra-phenolate complexes: Synthesis, structural studies and ethylene homo-(co-)polymerization capability. *RSC Adv.* **2015**, *5*, 89783–89796. [CrossRef]
35. Redshaw, C.; Walton, M.J.; Lee, D.S.; Jiang, C.; Elsegood, M.R.J.; Michiue, K. Vanadium(V) Oxo and Imido Calix[8]arene Complexes: Synthesis, Structural Studies, and Ethylene Homo/Copolymerisation Capability. *Chem.-Eur. J.* **2015**, *21*, 5199–5210. [CrossRef]
36. Diteepeng, N.; Tang, X.; Hou, X.; Li, Y.-S.; Phomphrai, K.; Nomura, K. Ethylene polymerisation and ethylene/norbornene copolymerisation by using aryloxo-modified vanadium(v) complexes containing 2,6-difluoro-, dichloro-phenylimido complexes. *Dalton Trans.* **2015**, *44*, 12273–12281. [CrossRef]
37. Zanchin, G.; Bertini, F.; Vendier, L.; Ricci, G.; Lorber, C.; Leone, G. Copolymerization of ethylene with propylene and higher α-olefins catalyzed by (imido)vanadium(iv) dichloride complexes. *Polym. Chem.* **2019**, *10*, 6200–6216. [CrossRef]
38. Ochędzan-Siodłak, W.; Siodłak, D.; Banaś, K.; Halikowska, K.; Wierzba, S.; Doležal, K. Naturally Occurring Oxazole Structural Units as Ligands of Vanadium Catalysts for Ethylene-Norbornene (Co)polymerization. *Catalysts* **2021**, *11*, 923. [CrossRef]

39. Wu, R.; Niu, Z.; Huang, L.; Yang, Y.; Xia, Z.; Fan, W.; Dai, Q.; Cui, L.; He, J.; Bai, C. Thermally stable vanadium complexes supported by the iminophenyl oxazolinylphenylamine ligands: Synthesis, characterization and application for ethylene (co-)polymerization. *Dalton Trans.* **2021**, *50*, 16067–16075. [CrossRef]
40. Białek, M.; Fryga, J.; Spaleniak, G.; Matsko, M.A.; Hajdasz, N. Ethylene homo- and copolymerization catalyzed by vanadium, zirconium, and titanium complexes having potentially tridentate Schiff base ligands. *J. Catal.* **2021**, *400*, 184–194. [CrossRef]
41. Nie, J.; Ren, F.; Li, Z.; Tian, K.; Zou, H.; Hou, X. Design and synthesis of binuclear vanadium catalysts for copolymerization of ethylene and polar monomers. *Polym. Chem.* **2022**, *13*, 3876–3881. [CrossRef]
42. Ge, F.; Dan, Y.; Al-Khafaji, Y.; Prior, T.J.; Jiang, L.; Elsegood, M.R.J.; Redshaw, C. Vanadium(v) phenolate complexes for ring opening homo- and co-polymerisation of ε-caprolactone, l-lactide and rac-lactide. *RSC Adv.* **2016**, *6*, 4792–4802. [CrossRef]
43. Białek, M.; Fryga, J.; Spaleniak, G.; Dziuk, B. Ring opening polymerization of ε-caprolactone initiated by titanium and vanadium complexes of ONO-type schiff base ligand. *J. Polym. Res.* **2021**, *28*, 79. [CrossRef]
44. Arbaoui, A.; Redshaw, C.; Homden, D.M.; Wright, J.A.; Elsegood, M.R.J. Vanadium-based imido-alkoxide pro-catalysts bearing bisphenolate ligands for ethylene and ε-caprolactone polymerisation. *Dalton Trans.* **2009**, 8911–8922. [CrossRef] [PubMed]
45. Clowes, L.; Redshaw, C.; Hughes, D.L. Vanadium-Based Pro-Catalysts Bearing Depleted 1,3-Calix[4]arenes for Ethylene or ε-Caprolactone Polymerization. *Inorg. Chem.* **2011**, *50*, 7838–7845. [CrossRef] [PubMed]
46. Clowes, L.; Walton, M.; Redshaw, C.; Chao, Y.; Walton, A.; Elo, P.; Sumerin, V.; Hughes, D.L. Vanadium(iii) phenoxyimine complexes for ethylene or ε-caprolactone polymerization: Mononuclear versus binuclear pre-catalysts. *Catal. Sci. Technol.* **2013**, *3*, 152–160. [CrossRef]
47. Ma, J.; Zhao, K.-Q.; Walton, M.; Wright, J.A.; Hughes, D.L.; Elsegood, M.R.J.; Michiue, K.; Sun, X.; Redshaw, C. Tri- and tetra-dentate imine vanadyl complexes: Synthesis, structure and ethylene polymerization/ring opening polymerization capability. *Dalton Trans.* **2014**, *43*, 16698–16706. [CrossRef] [PubMed]
48. Xing, T.; Prior, T.J.; Elsegood, M.R.J.; Semikolenova, N.V.; Soshnikov, I.E.; Bryliakov, K.P.; Chen, K.; Redshaw, C. Vanadium complexes derived from oxacalix[6]arenes: Structural studies and use in the ring opening homo-/co-polymerization of ε-caprolactone/δ-valerolactone and ethylene polymerization. *Catal. Sci. Technol.* **2021**, *11*, 624–636. [CrossRef]
49. Ishikura, H.; Neven, R.; Lange, T.; Galetová, A.; Blom, B.; Romano, D. Developments in vanadium-catalysed polymerisation reactions: A review. *Inorg. Chim. Acta* **2021**, *515*, 120047. [CrossRef]
50. Cusi, K.; Cukier, S.; DeFronzo, R.A.; Torres, M.; Puchulu, F.M.; Redondo, J.C.P. Vanadyl Sulfate Improves Hepatic and Muscle Insulin Sensitivity in Type 2 Diabetes. *J. Clin. Endocrinol. Metab.* **2001**, *86*, 1410–1417. [CrossRef]
51. Redshaw, C.; Elsegood, M.R.J.; Wright, J.A.; Baillie-Johnson, H.; Yamato, T.; De Giovanni, S.; Mueller, A. Cellular uptake of a fluorescent vanadyl sulfonylcalix[4]arene. *Chem. Commun.* **2012**, *48*, 1129–1131. [CrossRef]
52. Suzuki, N.; Kobayashi, G.; Hasegawa, T.; Masuyama, Y. Syntheses and structures of titanium complexes having O,N,O-tridentate ligands and their catalytic ability for ethylene polymerization. *J. Organomet. Chem.* **2012**, *717*, 23–28. [CrossRef]
53. Lai, F.-J.; Huang, T.-W.; Chang, Y.-L.; Chang, H.-Y.; Lu, W.-Y.; Ding, S.; Chen, H.-Y.; Chiu, C.-C.; Wu, K.-H. Titanium complexes bearing 2,6-Bis(o-hydroxyalkyl)pyridine ligands in the ring-opening polymerization of L-Lactide and ε-caprolactone. *Polymer* **2020**, *204*, 122860. [CrossRef]
54. Nakayama, Y.; Ikushima, N.; Nakamura, A. *Cis*-Specific Polymerization of Norbornene Catalyzed by Tungsten Based Complex Catalysts Bearing an O–N–O Tridentate Ligand. *Chem. Lett.* **1997**, *26*, 861–862. [CrossRef]
55. Evans, W.J.; Anwander, R.; Berlekamp, U.H.; Ziller, J.W. Synthesis and Structure of Lanthanide Complexes Derived from the O,N-Chelating, Bis(methylpyridine)-Substituted Alcohol HOC(CMe3)(2-CH2NC5H3Me-6)2. *Inorg. Chem.* **1995**, *34*, 3583–3588. [CrossRef]
56. Gibson, V.C.; Newton, C.; Redshaw, C.; Solan, G.A.; White, A.J.P.; Williams, D.J. Low valent chromium complexes bearing N,O-chelating pyridyl-enolate ligands $[OC(Bu^t)(=2\text{-}CHN_5H_3Me\text{-}x)]^-$ (x = 3–6). *Dalton Trans.* **2003**, 4612–4617. [CrossRef]
57. Berg, J.M.; Holm, R.H. Model for the active site of oxo-transfer molybdoenzymes: Synthesis, structure, and properties. *J. Am. Chem. Soc.* **1985**, *107*, 917–925. [CrossRef]
58. Addison, A.W.; Rao, T.N.; Reedijk, J.; van Rijn, J.; Verschoor, G.C. Synthesis, structure, and spectroscopic properties of copper(II) compounds containing nitrogen–sulphur donor ligands; the crystal and molecular structure of aqua[1,7-bis(N-methylbenzimidazol-2′-yl)-2,6-dithiaheptane]copper(II) perchlorate. *J. Chem. Soc. Dalton Trans.* **1984**, *7*, 1349–1356. [CrossRef]
59. Li, H.; Wang, C.; Bai, F.; Yue, J.; Woo, H.-G. Living Ring-Opening Polymerization of l-Lactide Catalyzed by Red-Al. *Organometallics* **2004**, *23*, 1411–1415. [CrossRef]
60. Soshnikov, I.E.; Semikolenova, N.V.; Shubin, A.A.; Bryliakov, K.P.; Zakharov, V.A.; Redshaw, C.; Talsi, E.P. EPR Monitoring of Vanadium(IV) Species Formed upon Activation of Vanadium(V) Polyphenolate Precatalysts with AlR_2Cl and AlR_2Cl/Ethyltrichloroacetate (R = Me, Et). *Organometallics* **2009**, *28*, 6714–6720. [CrossRef]
61. Soshnikov, I.E.; Semikolenova, N.V.; Bryliakov, K.P.; Shubin, A.A.; Zakharov, V.A.; Redshaw, C.; Talsi, E.P. An EPR Study of the V(IV) Species Formed Upon Activation of a Vanadyl Phenoxyimine Polymerization Catalyst with $AlR_3$and AlR_2Cl (R = Me, Et). *Macromol. Chem. Phys.* **2009**, *210*, 542–548. [CrossRef]
62. Soshnikov, I.E.; Semikolenova, N.V.; Bryliakov, K.; Zakharov, V.A.; Redshaw, C.; Talsi, E.P. An EPR study of the vanadium species formed upon interaction of vanadyl N and C-capped tris(phenolate) complexes with $AlEt_3$ and $AlEt_2Cl$. *J. Mol. Catal. A Chem.* **2009**, *303*, 23–29. [CrossRef]

63. Deng, S.; Liu, Z.; Liu, B.; Jin, Y. Unravelling the Role of Al-alkyl Cocatalyst for the VO_x/SiO_2 Ethylene Polymerization Catalyst: Diethylaluminum Chloride vs. Triethylaluminum. *ChemCatChem* **2021**, *13*, 2278–2292. [CrossRef]
64. Manzer, L. Tetrahydrofuran Complexes of Selected Early Transition-Metals. In *Inorganic Syntheses*; Fackler, J.P., Ed.; John Wiley & Sons: Hoboken, NJ, USA, 1982; Volume 21, pp. 135–140. ISBN 978-0-470-13287-6.
65. Edema, J.J.H.; Stauthamer, W.; Van Bolhuis, F.; Gambarotta, S.; Smeets, W.J.J.; Spek, A.L. Novel vanadium(II) amine complexes: A facile entry in the chemistry of divalent vanadium. Synthesis and characterization of mononuclear L4VCl2 [L = amine, pyridine]: X-ray structures of trans-(TMEDA)2VCl2 [TMEDA = N,N,N′,N′-tetramethylethylenediamine] and trans-Mz2V(py)2 [Mz = o-C6H4CH2N(CH3)2, py = pyridine]. *Inorg. Chem.* **1990**, *29*, 1302–1306. [CrossRef]
66. Sheldrick, G.M. SHELXT-Integrated Space-Group and Crystal-Structure Determination. *Acta Crystallogr. Sect. A* **2015**, *A71*, 3–8. [CrossRef]
67. Sheldrick, G.M. Crystal Structure Refinement with SHELXL. *Acta Crystallogr. C* **2015**, *C71*, 3–8. [CrossRef]